J MATER RES TECHNOL. 2016;xxx(xx):xxx–xxx

Available online at www.sciencedirect.com

jmr&t Journal of Materials Research and Technology

www.jmrt.com.br

Original Article

Electrochemical corrosion study of Mg–Al–Zn–Mn alloy in aqueous ethylene glycol containing chloride ions

Harish Medhashree, Adka Nityananda Shetty *

Department of Chemistry, National Institute of Technology Karnataka, Surathkal, Srinivasnagar 575 025, Karnataka, India

ARTICLE INFO

Article history:
Received 24 July 2015
Accepted 12 April 2016
Available online xxx

Keywords:
Mg–Al–Zn–Mn alloy
Ethylene glycol
Cyclic polarization
EIS
EDX
SEM

ABSTRACT

Nowadays most of the automobiles use magnesium alloys in the components of the engine coolant systems. These engine coolants used are mainly composed of aqueous ethylene glycol along with some inhibitors. Generally the engine coolants are contaminated by environmental anions like chlorides, which would enhance the rate of corrosion of the alloys used in the coolant system. In the present study, the corrosion behavior of Mg–Al–Zn–Mn alloy in 30% (v/v) aqueous ethylene glycol containing chloride anions at neutral pH was investigated. Electrochemical techniques, such as potentiodynamic polarization method, cyclic polarization and electrochemical impedance spectroscopy (EIS) were used to study the corrosion behavior of Mg–Al–Zn–Mn alloy. The surface morphology, microstructure and surface composition of the alloy were studied by using the scanning electron microscopy (SEM), optical microscopy and energy dispersion X-ray (EDX) analysis, respectively. Electrochemical investigations show that the rate of corrosion increases with the increase in chloride ion concentration and also with the increase in medium temperature.

1. Introduction

In recent years, magnesium alloys have inspired a great interest as eco-friendly structural materials for automobiles and aircrafts due to their properties like high strength to weight ratio, low cost of production, ease of machinability, high damping capacity, castability, weldability and recyclability [1,2]. Apart from these well-known applications, magnesium alloys find their utility as orthopedic biomaterials because of their non-toxicity, lighter density than implant materials, greater fracture toughness compared to hydroxyapatite, similar elastic modulus and compressive yield strength values as that of natural bone and good biocompatibility. Lightweight and excellent damping characteristics of magnesium alloys make them a popular material choice in sport equipments. Magnesium alloys have great heat transfer property, ability to shield electromagnetic interference and radio frequency

* *Corresponding author*.
E-mail: nityashreya@gmail.com (A.N. Shetty).

http://dx.doi.org/10.1016/j.jmrt.2016.04.003

Please cite this article in press as: Medhashree H, Shetty AN. Electrochemical corrosion study of Mg–Al–Zn–Mn alloy in aqueous ethylene glycol containing chloride ions. J Mater Res Technol. 2016. http://dx.doi.org/10.1016/j.jmrt.2016.04.003

interference, etc., making them promising materials for electronic applications [3]. But the poor corrosion resistance is their limitation in complete utilization. The poor corrosion resistance is due to the less protective hydroxide film formed on the surface, which is having Pilling–Bedworth ratio ~0.81 and also due to the presence of secondary phase which leads to galvanic corrosion [4,5].

Magnesium alloys are mainly classified into two major alloying systems. The alloys containing aluminum (2–10%) with minor addition of zinc and manganese, find applications in the temperature range of 95–125 °C. The second group of alloys containing various elements such as rare earths, zinc, thorium and silver, but not aluminum, have improved elevated temperature properties compared to the alloys which contains aluminum as major alloying element [6]. The most widely used Mg–Al alloy is Mg–Al–Zn–Mn alloy containing minor addition of Zn and Mn. Aluminum increases the corrosion resistance property of the alloy by altering the composition of the hydroxide film formed on the surface. Zinc increases the tolerance limit of iron, copper and nickel. Similarly, manganese improves the corrosion resistance property of the alloy, as well as it reduces the effect of impurities when their tolerance limits were exceeded. The influence of 14 different elements on the corrosion behavior of magnesium alloy in salt water was studied by Hanawalt et al. and it was discovered that Fe, Co, Ni and Cu had a profound accelerating influence on the corrosion behavior [1]. Considerable amounts of research have been carried out for improving the corrosion resistance property of the magnesium alloy by adding various elements and by different techniques [7–12].

The reports are available in the literature on the corrosion behavior of magnesium alloys in various aqueous media containing different concentration of sodium chloride, sodium borate buffer, sodium sulfate, acidic, neutral and basic buffer, sodium bicarbonate, simulated biological fluid, etc. [2,13–20]. But a very few investigations are available in aqueous organic medium like ethylene glycol, which finds significance in automotive industries. Nowadays, most of the automotive industries use magnesium alloys in engine cooling system components and the major composition of conventional coolant is 30 vol% to 70 vol% ethylene glycol. Corrosion of engine components by the coolant is a major issue in automotive industries. Song and St. John have reported the studies on the corrosion behavior of pure magnesium in ethylene glycol solution. They have explained the effect of NaCl, $NaHCO_3$ and Na_2SO_4 on the corrosion behavior of pure magnesium [21]. Slavcheva and Schmitt have investigated the corrosion behavior of AZ91 magnesium alloy in 50 wt.% aqueous ethylene glycol by electrochemical methods [22]. Electrochemical corrosion behavior of AZ91D alloy in 30% aqueous ethylene glycol and the effect of NaCl and NaF were studied by Fekry and Fatayerji using potentiodynamic polarization and electrochemical impedance measurements [23]. Huang et al. have studied the galvanic corrosion behavior of GW103 and AZ91D alloy in ethylene glycol solution at ambient and elevated temperatures [24]. Slavcheva et al. have investigated the effect of chloride ions in 50 wt.% aqueous solution of ethylene glycol on the corrosion behavior of AZ91 magnesium alloy [25]. In the present study it is intended to investigate the effect of chloride ions concentration and temperature on the corrosion behavior of Mg–Al–Zn–Mn alloy in 30% (v/v) aqueous ethylene glycol using electrochemical corrosion monitoring techniques.

2. Experimental

2.1. Material and medium

The specimen under study, the Mg–Al–Zn–Mn alloy, was analyzed by atomic absorption spectroscopy (AAS TIFAC GBC 932 plus) and it has the composition as listed in Table 1. Cylindrical test coupon was mounted in epoxy resin to get a constant exposed area of 0.834 cm^2. This exposed area was ground by using emery papers of different grade (600–2000). After grinding with emery papers, the surface was polished on a polishing wheel using legated alumina as abrasive to get a mirror finish. Then the specimen was washed with double distilled water and degreased with acetone. The specimen was dried properly before immersing in the corrosive medium.

Analytical grade sodium chloride, double distilled water and analytical grade ethylene glycol were used to prepare the electrolyte medium of 30% (v/v) aqueous ethylene glycol solution containing 2 mM, 4 mM, 6 mM, 8 mM and 10 mM chloride anions. All the experiments were carried out in a calibrated thermostat at temperatures of 30 °C, 35 °C, 40 °C, 45 °C and 50 °C (±0.5 °C) under unstirred conditions.

2.2. Electrochemical measurements

An electrochemical work station, Gill AC having ACM instrument Version 5 software was used for all the electrochemical measurements. Conventional three electrodes compartment Pyrex glass cell with platinum as counter electrode, saturated calomel electrode as reference and Mg–Al–Zn–Mn alloy as working electrode were used. The polarization studies were carried out immediately after the EIS studies on the same exposed electrode surface without any additional surface treatment.

2.2.1. Potentiodynamic polarization studies

A steady state open circuit potential (OCP) was established by immersing the working electrode in the medium and then it was polarized by applying a potential drift of −250 mV cathodically and +250 mV anodically with respect to the OCP, at a scan rate of 1 mV s^{-1}.

2.2.2. Cyclic polarization

The cyclic polarization measurements were carried out after the attainment of steady state open circuit potential for 15 min. The electrode was subjected to a cyclic potential ramp starting from −1.8 V to −1.3 V, and then a reverse scan from −1.3 V to −1.8 V, both at a scan rate of 1 mV s^{-1}.

2.2.3. Electrochemical impedance spectroscopy (EIS) studies

Impedance measurements were carried out at the open circuit potential by the application of a periodic small amplitude of 10 mV over a wide range of frequencies from 100 kHz to

Please cite this article in press as: Medhashree H, Shetty AN. Electrochemical corrosion study of Mg–Al–Zn–Mn alloy in aqueous ethylene glycol containing chloride ions. J Mater Res Technol. 2016. http://dx.doi.org/10.1016/j.jmrt.2016.04.003

Table 1 – Composition of the Mg–Al–Zn–Mn alloy.

Element	Al	Zn	Mn	Si	Cu	Fe	Mg
Composition (wt.%)	8.30	0.60	0.35	0.20	0.12	0.20	Balance

0.01 Hz. Nyquist plots were used to analyze the impedance data.

In all the above electrochemical measurements, at least three similar results were considered and average values have been reported.

2.3. *Surface characterization*

The surface morphology and surface composition of the freshly polished and corroded surfaces were studied by recording the SEM images using JEOL JSM-6380LA analytical scanning electron microscope. The corresponding EDX spectra were subsequently recorded. Optical microscope Zeiss AXIO Lab. A1 was used to record the optical image after etching the specimen in acetic-picral. Etching reagent was prepared by using 5 mL of acetic acid, 6 g of picric acid, 10 mL of water and 100 mL of ethanol. The alloy surface was etched to reveal the microstructure of the Mg–Al–Zn–Mn alloy [26].

3. Results and discussions

3.1. *Potentiodynamic polarization measurements*

The potentiodynamic polarization measurements for the corrosion of Mg–Al–Zn–Mn alloy specimen were carried out in 30% (v/v) aqueous ethylene glycol containing different concentrations of chloride ions at different solution temperatures. Fig. 1 shows the potentiodynamic polarization curves for the corrosion of Mg–Al–Zn–Mn alloy in 30% (v/v) aqueous ethylene glycol containing different concentration of chloride ions at 50 °C. Similar curves were obtained at other temperatures also.

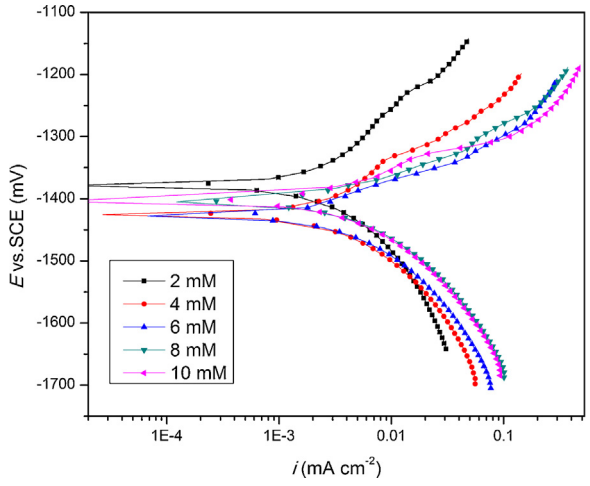

Fig. 1 – Potentiodynamic polarization plots for the corrosion of Mg–Al–Zn–Mn alloy in 30% aqueous ethylene glycol containing different concentrations of the chloride ions at 50 °C.

From Fig. 1, it is clear that the polarization curves are shifted to higher current density region with the increase in chloride ion concentration. The anodic polarization curves, representing the anodic dissolution of the magnesium alloy show inflection points characterized by two different slopes at potentials more positive than corrosion potential. This results from some sort of kinetic barrier effect, most probably by the deposition of corrosion product surface film followed by its dissolution at increased anodic overvoltage [27,28]. The cathodic polarization curves are characterized with distinctly linear Tafel regions, and they represent the hydrogen evaluation reactions through the reduction of water [29]. The overall shapes of the polarization curves remain the same in the presence of different concentrations of chloride ions, which indicate no change in the corrosion mechanism as the concentration of chloride ions changes. The catholic polarization curves were used to measure the electrochemical parameters by extrapolating the linear Tafel regions of the curves to the OCP, as the anodic curves do not possess distinct linear Tafel regions. The potentiodynamic polarization parameters, such as corrosion current density (i_{corr}), corrosion potential (E_{corr}) and cathodic slope (b_c) are tabulated in Table 2.

The corrosion rate (υ_{corr}) was calculated using the following Eq. (1) [30].

$$\upsilon_{corr} = \frac{K \times i_{corr} \times EW}{\rho} \quad (1)$$

where, $K = 0.00327$ is a constant, which defines the unit of corrosion rate (mm y^{-1}), i_{corr} is the current density ($\mu A\,cm^{-2}$), ρ is the density of the specimen, EW is the equivalent weight of the alloy, which is calculated using Eq. (2).

$$EW = \frac{1}{\sum \left[\frac{n_i \times f_i}{W_i}\right]} \quad (2)$$

where f_i is the weight fraction of the ith element of the alloy, W_i is the atomic weight of the ith element of the alloy and n_i is the valence of the ith element of the alloy [30].

From Table 2 it is evident that the rate of corrosion increases with the increase in chloride ion concentration. This is attributed to the dissolution of the partially formed $Mg(OH)_2$ film in the presence of chloride ions as $MgCl_2$, which is having more solubility than $Mg(OH)_2$ film [31]. Several studies have established that chloride is an effective corrosive for magnesium and its alloys [2,13,19,17].

The corrosion of magnesium alloys in aqueous medium proceeds through an electrochemical reaction between magnesium and water to produce magnesium hydroxide and hydrogen as per the following Eq. (3):

$$Mg + 2H_2O \rightarrow Mg(OH)_2 + H_2 \quad (3)$$

Please cite this article in press as: Medhashree H, Shetty AN. Electrochemical corrosion study of Mg–Al–Zn–Mn alloy in aqueous ethylene glycol containing chloride ions. J Mater Res Technol. 2016. http://dx.doi.org/10.1016/j.jmrt.2016.04.003

Table 2 – Potentiodynamic polarization and electrochemical impedance parameters for the corrosion of Mg–Al–Zn–Mn alloy in 30% (v/v) aqueous ethylene glycol containing different concentrations of chloride ions at different temperatures.

Concentration of Cl^- (mM)	Temperature (°C)	E_{corr} vs SCE (mV)	$-b_c$ (mV dec^{-1})	i_{corr} ($\mu A\,cm^{-2}$)	υ_{corr} (mm y^{-1})	R_{hf} (ohm cm^2)
2	30	−1476	356	4.582	0.098	7613
	35	−1466	363	5.357	0.115	6296
	40	−1486	332	6.024	0.129	5273
	45	−1470	370	6.786	0.146	5138
	50	−1379	442	7.852	0.169	4078
4	30	−1504	282	5.947	0.128	5913
	35	−1430	300	7.534	0.161	5044
	40	−1452	296	8.394	0.180	4455
	45	−1423	316	9.232	0.198	4025
	50	−1426	343	10.215	0.219	3640
6	30	−1499	270	6.849	0.147	5762
	35	−1445	279	9.531	0.205	4372
	40	−1433	297	10.588	0.228	3272
	45	−1420	317	11.6789	0.251	3173
	50	−1428	338	12.823	0.276	3061
8	30	−1410	279	7.705	0.166	5429
	35	−1440	240	10.433	0.224	4294
	40	−1470	337	11.686	0.251	3178
	45	−1452	302	12.011	0.258	2970
	50	−1406	296	13.172	0.283	2649
10	30	−1458	286	10.093	0.217	5304
	35	−1446	269	11.175	0.240	4024
	40	−1416	310	12.272	0.264	3048
	45	−1461	306	13.050	0.280	2853
	50	−1405	339	15.370	0.330	2686

The anodic dissolution of magnesium is considered to be proceeding through the oxidation of magnesium into monovalent Mg^+ ions and divalent Mg^{2+} ions as summarized by the following reactions, represented in Eqs. (4) and (5) [32].

$$Mg \rightarrow Mg^+ + e^- \quad (4)$$

$$Mg \rightarrow Mg^{2+} + 2e^- \quad (5)$$

The steady state working potential of magnesium is about −1.5 V, even though the standard electrode potential of magnesium is −2.38 V. The difference in potential has been attributed to the formation of $Mg(OH)_2$ film on the metal surface [33]. The anodic dissolution of magnesium and its alloys involves two oxidation processes as represented in Eqs. (4) and (5). At more active potentials around −2.78 V (vs SCE) magnesium is oxidized to monovalent magnesium ion and at slightly higher potentials of −1.56 V (vs SCE) oxidation to divalent magnesium ion takes place in parallel with the former oxidation [34]. As the monovalent magnesium ion is unstable, undergoes oxidation to divalent magnesium ion through a series of reactions involving unstable intermediates like magnesium hydride as shown in Eqs. (6)–(9) below:

$$Mg^+ + 2H^+ + 3e^- \rightarrow MgH_2 \quad (6)$$

$$MgH_2 + 2H_2O \rightarrow Mg^{2+} + 2OH^- + 2H_2 \quad (7)$$

$$Mg^{2+} + 2OH^- \rightarrow Mg(OH)_2 \quad (8)$$

$$2Mg^+ + 2H_2O \rightarrow Mg^{2+} + Mg(OH)_2 + H_2 \quad (9)$$

Mg–Al–Zn–Mn alloys are dual phase alloys with a typical microstructure of having a primary α-phase and a divorced eutectic β-phase, distributed along the grain boundaries [35]. The α-Mg matrix is α-Mg–Al–Zn solid solution with the same crystal structure as pure magnesium and the β-phase is with a composition of $Mg_{17}Al_{12}$. They are also found to have inter metallic inclusions of $MnAl_2$ [2]. The α-Mg matrix with a very negative free corrosion potential acts as anodic with respect to the β-phase of $Mg_{17}Al_{12}$, undergoes corrosion by micro galvanic coupling between anodic α-Mg phase and cathodic β-$Mg_{17}Al_{12}$ phase [7,36–41]. However, the β-$Mg_{17}Al_{12}$ phase may act as a barrier against corrosion propagation if it is in the form of a continuous network [37,38]. The corrosion of the alloy in the aqueous ethylene glycol media in the presence of chloride ions indicates the discontinuities in the β-phase. According to the results published in the literature, magnesium alloys exhibit higher corrosion resistance than pure magnesium [16]. The improvement of the corrosion behavior of Mg alloys in the presence of alloying elements has been attributed to a number of factors such as refining of the β-phase and formation of more continuous network, suppression of β-phase formation by forming another intermetallic, which is less harmful to the α-Mg matrix, and incorporation of the added elements into the protective film and thus increasing its stability [9,42,43]. Small additions of Mn have been reported to increase the corrosion resistance of magnesium alloys and reduce the effects of metallic impurities [44,45].

Please cite this article in press as: Medhashree H, Shetty AN. Electrochemical corrosion study of Mg–Al–Zn–Mn alloy in aqueous ethylene glycol containing chloride ions. J Mater Res Technol. 2016. http://dx.doi.org/10.1016/j.jmrt.2016.04.003

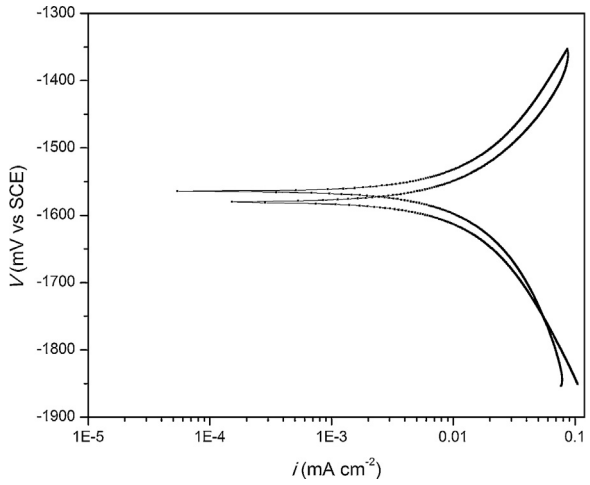

Fig. 2 – Cyclic polarization curve for the corrosion of Mg–Al–Zn–Mn alloy in 30% (v/v) aqueous ethylene glycol containing 4 mM chloride ions at 30 °C.

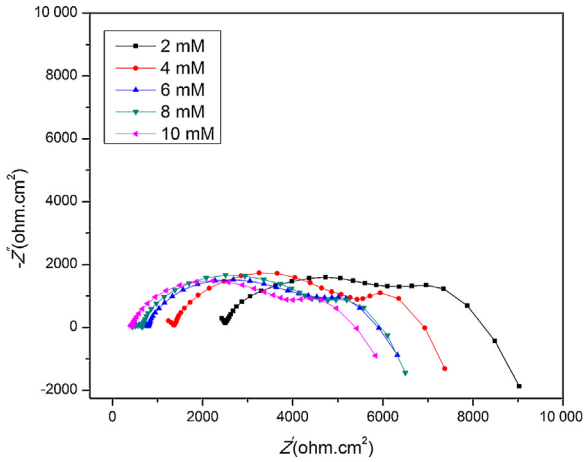

Fig. 4 – Nyquist plots for the corrosion of Mg–Al–Zn–Mn alloy in 30% (v/v) aqueous solution of ethylene glycol containing different concentration of chloride ions at 40 °C.

3.2. *Cyclic polarization*

The cyclic polarization curves are generally used to study the pitting corrosion in corrosive environment. The forward scan represents the polarization behavior of the non-corroded areas, while the reverse scan is associated with the corroded areas [46]. The cyclic polarization curve for the corrosion of Mg–Al–Zn–Mn alloy in 30% (v/v) aqueous ethylene glycol containing 4 mM chloride ions at 30 °C is as shown in Fig. 2. The corrosion potential on the forward scan is −1.564 V and that on the reverse scan is −1.579 V. The corrosion potential on the reverse scan is more negative than the forward scan, which indicates that corroded area still acts as anode for further galvanic corrosion and protects the non-corroded area as cathode, resulting in accelerated corrosion in the corroded area, causing the formation of pits [47]. The formation of visible pits on the surface of the alloy is as shown in Fig. 3.

3.3. *Electrochemical impedance spectroscopy (EIS)*

Electrochemical impedance spectroscopy is a non-destructive technique which provides minimal perturbative signal and can be used to study the response of corroding electrodes to small amplitude alternating potential signals of largely varying frequencies [48]. Fig. 4 shows the Nyquist plots for the corrosion of Mg–Al–Zn–Mn alloy in 30% (v/v) aqueous ethylene glycol containing different concentrations of chloride ions at 40 °C. Similar plots were obtained at other temperatures also. The Nyquist plots consist of two capacitive loops at higher and medium frequencies and the beginning of an inductive loop at lower frequency region. The high frequency capacitive loop is attributed to the charge transfer of corrosion process and oxide film effects. The medium frequency capacitive loop represents mass transport as a consequence of diffusion or electrolyte ingress through corrosion product. The lower frequency inductive loop represents the relaxation of adsorbed species like $Mg(OH)^+$ and $Mg(OH)_2$ adsorbed at the metal surface [49–51]. Song and Xu have suggested that the medium frequency capacitive loop represents the combination of pseudo resistance and capacitance of the film formation and dissolution process [52]. From Fig. 4, it is clear that the diameter of the capacitive loop decreases with the increase in the concentration of chloride ions, indicating an increase in the corrosion rate with the increase in chloride ion concentration in the corrosion medium.

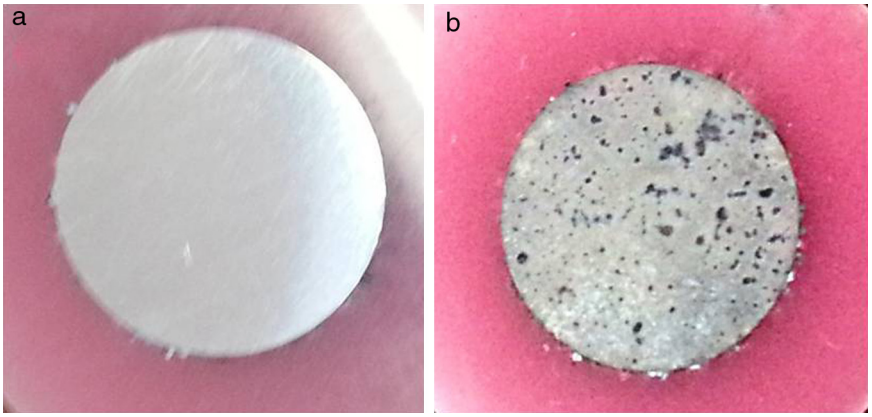

Fig. 3 – Optical photos of Mg–Al–Zn–Mn alloy surface (a) before cyclic polarization and (b) after cyclic polarization.

Please cite this article in press as: Medhashree H, Shetty AN. Electrochemical corrosion study of Mg–Al–Zn–Mn alloy in aqueous ethylene glycol containing chloride ions. J Mater Res Technol. 2016. http://dx.doi.org/10.1016/j.jmrt.2016.04.003

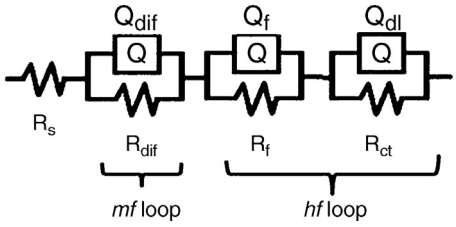

Fig. 5 – Equivalent electrical circuit used for the simulation of experimental impedance data points.

The equivalent circuit models derived by simulating the electrochemical behavior of the alloy-medium interface help in the best understanding of the impedance results. The circuit fitment for the obtained results was done by ZSimpWin software of version 3.21. The impedance data points neglecting the low frequency inductive loop, can be analyzed using an equivalent electrical circuit (EEC) as shown in Fig. 5. The simulation of impedance data points is presented in Fig. 6. The high frequency response can be simulated by a series of two parallel resistances – constant phase element (R-CPE) networks: the charge transfer resistance (R_{ct}) in parallel with the double layer CPE (Q_{dl}) and the resistance of the surface film (R_f) in parallel with the film CPE (Q_f). The resistance (R_{dif}) and CPE (Q_{dif}) associated with diffusion are assigned to the middle frequency response [53]. The constant phase element (Q_{dl}) is substituted for the ideal capacitive element to give a more accurate fit, as only by the introduction of constant phase element the lack of homogeneity and even porosity of the electrode surface can be accounted [9].

The impedance of the constant phase is given by the following Eq. (10):

$$Z_Q = Y_0^{-1}(j\omega)^{-n} \tag{10}$$

where Y_0 is the CPE constant, j is the imaginary number ($j^2 = -1$), ω is angular frequency and n is CPE exponent, which measures the heterogeneity or roughness of the surface. The value of $n = 1$ for ideal capacitor, $n = -1$ for ideal inductor and $n = 0$ for ideal resistor.

The capacitance and CPE are related by the following Eq. (11):

$$C = Y_0(\omega_m^n)^{n-1} \tag{11}$$

where ω_m^n is the frequency at which the imaginary part of the impedance ($Z^{//}$) has a maximum value.

The collective resistance associated with the high frequency loop (R_{hf}) is inversely related to the corrosion rate [54,55]. The values of R_{hf} for the corrosion of the alloy are listed in Table 2. It is evident from Table 2 that the corrosion rate increases with the increase in the concentration of chloride ions as indicated by the reduction in the R_{hf} values.

The capacitance of the double layer is related to the thickness of the double layer by the Helmholtz model Eq. (12):

$$C_{dl} = \frac{\varepsilon}{4\pi d} \tag{12}$$

where C_{dl} is the capacitance, ε is local dielectric constant and d is thickness of double layer [17].

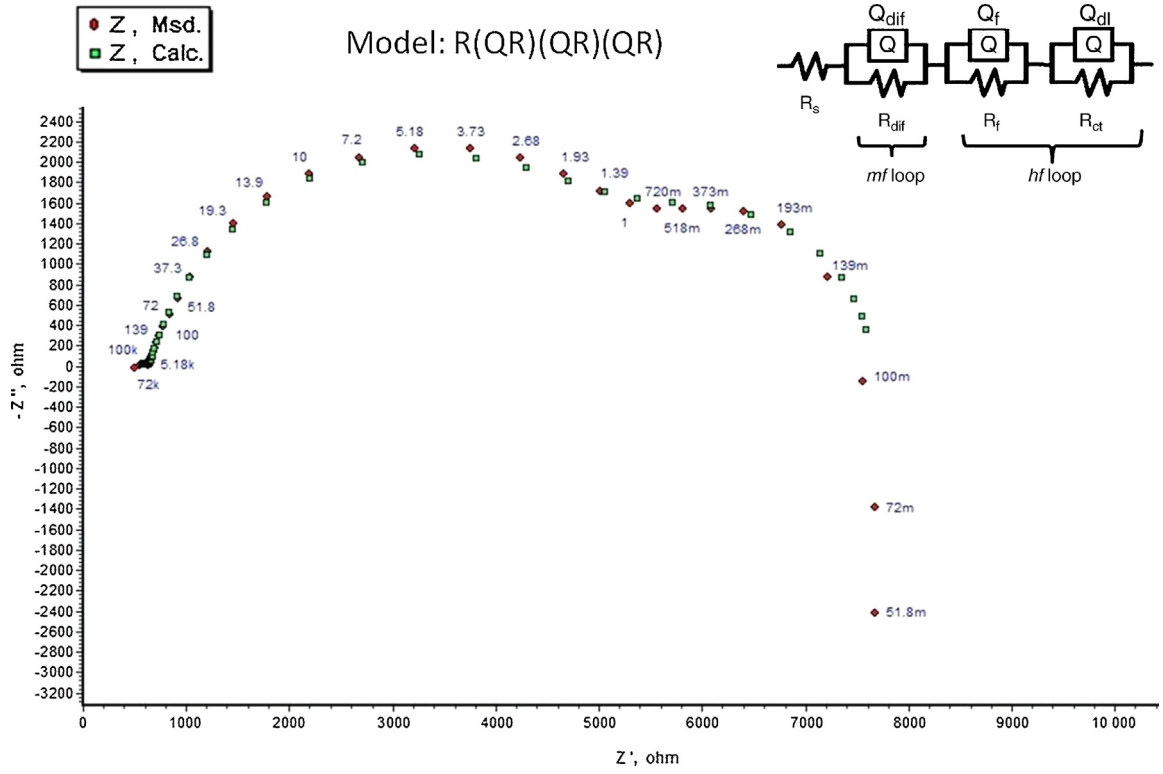

Fig. 6 – Simulation plot for the corrosion of Mg–Al–Zn–Mn alloy in 30% aqueous ethylene glycol containing 4 mM chloride ions at 45 °C.

Please cite this article in press as: Medhashree H, Shetty AN. Electrochemical corrosion study of Mg–Al–Zn–Mn alloy in aqueous ethylene glycol containing chloride ions. J Mater Res Technol. 2016. http://dx.doi.org/10.1016/j.jmrt.2016.04.003

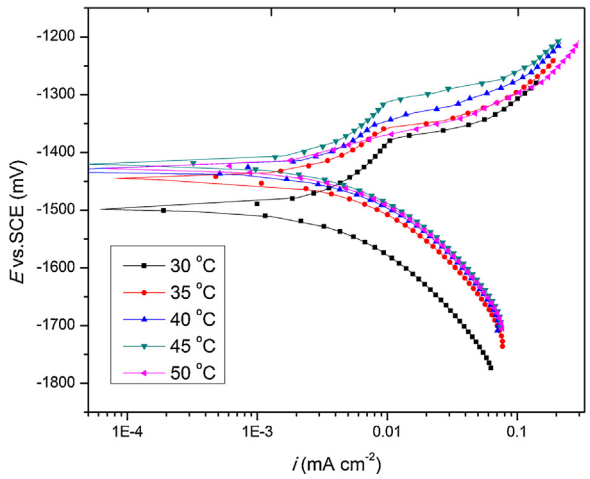

Fig. 7 – Potentiodynamic polarization plots for the corrosion of Mg–Al–Zn–Mn alloy in 30% aqueous ethylene glycol containing 6 mM chloride ions at different temperatures.

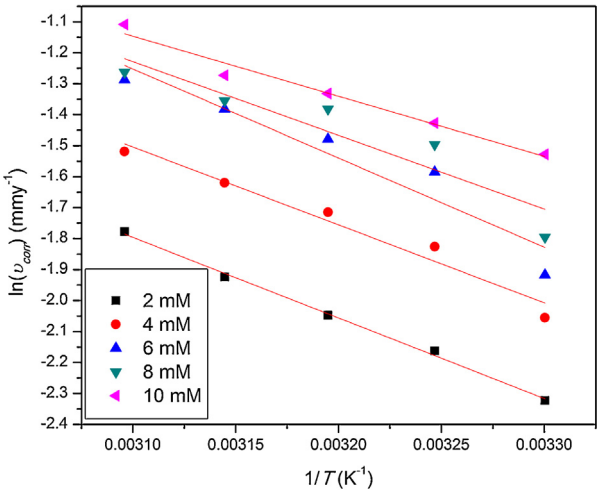

Fig. 9 – Arrhenius plots for the corrosion of Mg–Al–Zn–Mn alloy in 30% (v/v) ethylene glycol containing different concentration of chloride ions at different temperatures.

3.4. *Effect of temperature*

The effect of temperature on the corrosion of Mg–Al–Zn–Mn alloy was studied by measuring the corrosion rate at different temperatures in the range of 30–50 °C at an increment of 5 °C. Fig. 7 shows the potentiodynamic polarization curves for the corrosion of Mg–Al–Zn–Mn alloy in 30% aqueous ethylene glycol containing 6 mM chloride ions at different temperatures. Fig. 8 represents the Nyquist plots for the corrosion of Mg–Al–Zn–Mn alloy in 30% (v/v) aqueous solution of ethylene glycol containing 4 mM chloride ions at different temperatures. Similar plots were obtained in the presence of other concentrations of chloride ions also. From Fig. 7 it is seen that the polarization curves shifts to the higher current density region with the increase in temperature. In Fig. 8 the diameter of the Nyquist plots decreases with the increase in temperature. Both these facts indicate the increase in the rate of corrosion as the temperature is increased. The same trend is reflected in the results listed in Table 2, as the values of i_{corr} and υ_{corr} are observed to be increasing and the value of R_{hf} decreasing with the increase in temperature in a given medium. The shapes of the polarization curves and Nyquist plots remain unaltered with the change in temperature, indicating that the temperature alters only the rate of alloy corrosion but not the mechanism of corrosion.

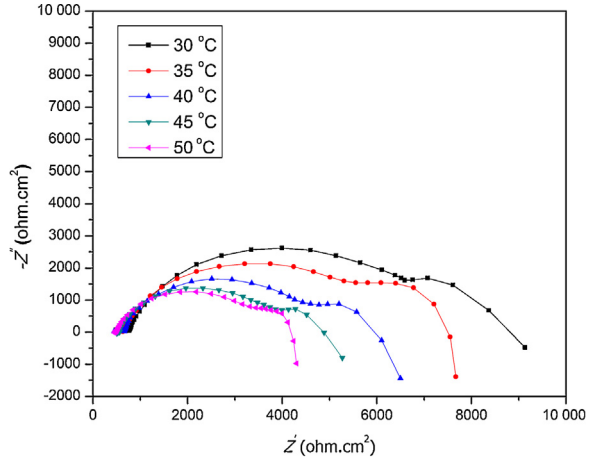

Fig. 8 – Nyquist plots for the corrosion of Mg–Al–Zn–Mn alloy in 30% (v/v) aqueous solution of ethylene glycol containing 4 mM chloride ions at different temperatures.

Arrhenius equation (Eq. (13)) was used to calculate the activation energy (E_a) of the corrosion process.

$$\ln(\upsilon_{corr}) = B - \left(\frac{E_a}{RT}\right) \tag{13}$$

where B is a constant, which depends on the type of the metal, R is the universal gas constant. The plot of $\ln(\upsilon_{corr})$ vs reciprocal of absolute temperature ($1/T$) gives a straight line. The activation energy values were calculated from the slope $= -E_a/R$. Fig. 9 shows the Arrhenius plots for the corrosion of Mg–Al–Zn–Mn alloy. The transition state theory equation (Eq. (14)) was used to calculate the enthalpy of activation ($\Delta H^{\#}$) and entropy of activation ($\Delta S^{\#}$).

$$\upsilon_{corr} = \left(\frac{RT}{Nh}\right) \exp\left(\frac{\Delta S^{\#}}{R}\right) \exp\left(\frac{-\Delta H^{\#}}{RT}\right) \tag{14}$$

where N is Avogadro's number and h is Plank's constant. A straight line graph is obtained by plotting $\ln(\upsilon_{corr}/T)$ vs $1/T$ (Fig. 10). Enthalpy of activation and entropy of activation were calculated from the slope $= -\Delta H^{\#}/R$ and intercept $= \ln(R/Nh) + \Delta S^{\#}/R$. The activation parameters for the corrosion process are listed in Table 3.

The E_a value, which is the measure of the energy barrier for the occurrence of corrosion reaction, in general, decreases with the increase in the concentration of chloride ions in the medium, indicating that corrosion of the alloy is thermodynamically more favored in the presence of higher concentration of chloride ions. The large negative values of

Please cite this article in press as: Medhashree H, Shetty AN. Electrochemical corrosion study of Mg–Al–Zn–Mn alloy in aqueous ethylene glycol containing chloride ions. J Mater Res Technol. 2016. http://dx.doi.org/10.1016/j.jmrt.2016.04.003

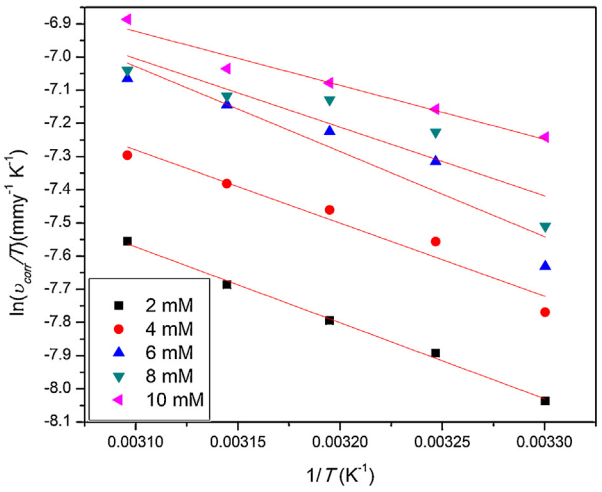

Fig. 10 – Plots of ($\ln v_{corr}/T$) vs 1/T for the corrosion of Mg–Al–Zn–Mn alloy in 30% (v/v) aqueous ethylene glycol containing different concentrations of chloride ions.

Table 3 – Activation parameters for the corrosion of Mg–Al–Zn–Mn alloy.

Concentration of Cl^- (mM)	E_a (kJ mol^{-1})	$\Delta H^{\#}$ (kJ mol^{-1})	$\Delta S^{\#}$ (J mol^{-1} K^{-1})
2	21.62	19.02	−201.52
4	20.91	18.31	−201.29
6	23.92	21.32	−189.87
8	19.78	17.18	−202.48
10	16.12	13.52	−213.15

$\Delta S^{\#}$ imply that the activated complex in the rate determining step is formed by association, resulting in a decrease in randomness on going from the reactants to the activated complex [56].

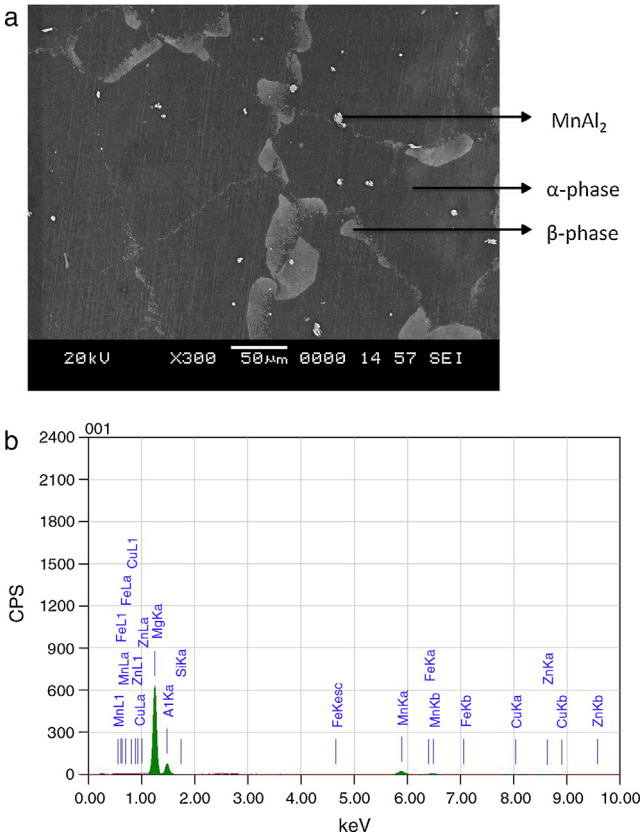

Fig. 11 – (a) SEM image and (b) EDX spectrum of a freshly polished surface of Mg–Al–Zn–Mn alloy, after etching in acetic-picral.

3.5. *Surface morphology*

The surface morphologies and surface compositions of the fresh and corroded alloy surfaces were analyzed by SEM and

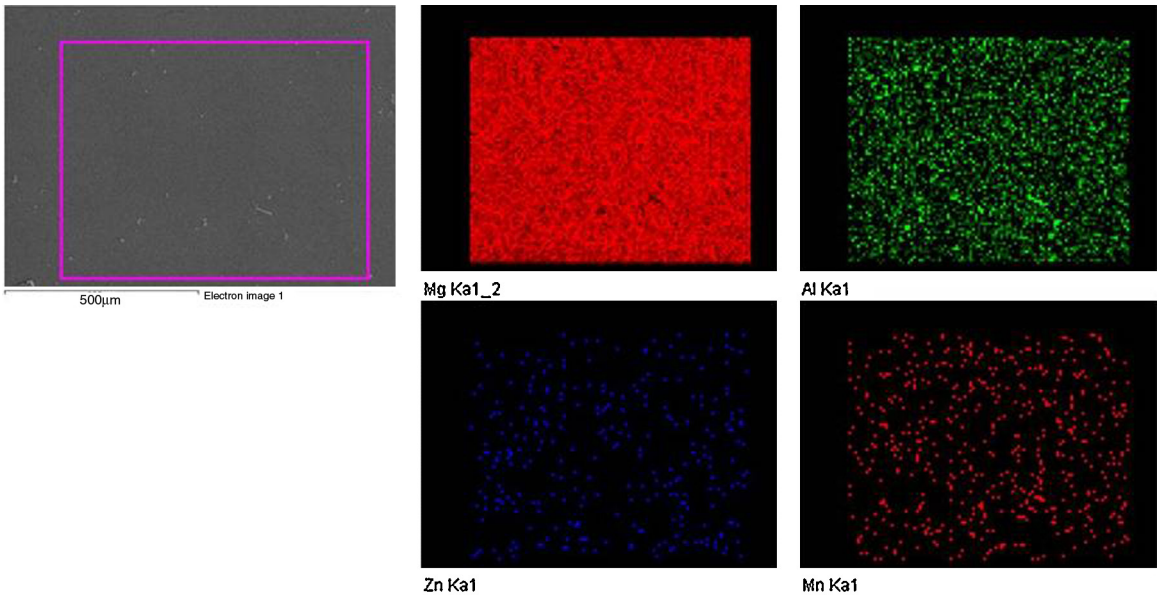

Fig. 12 – EDX mapping of Mg–Al–Zn–Mn alloy showing the distribution of various elements in the alloy.

Please cite this article in press as: Medhashree H, Shetty AN. Electrochemical corrosion study of Mg–Al–Zn–Mn alloy in aqueous ethylene glycol containing chloride ions. J Mater Res Technol. 2016. http://dx.doi.org/10.1016/j.jmrt.2016.04.003

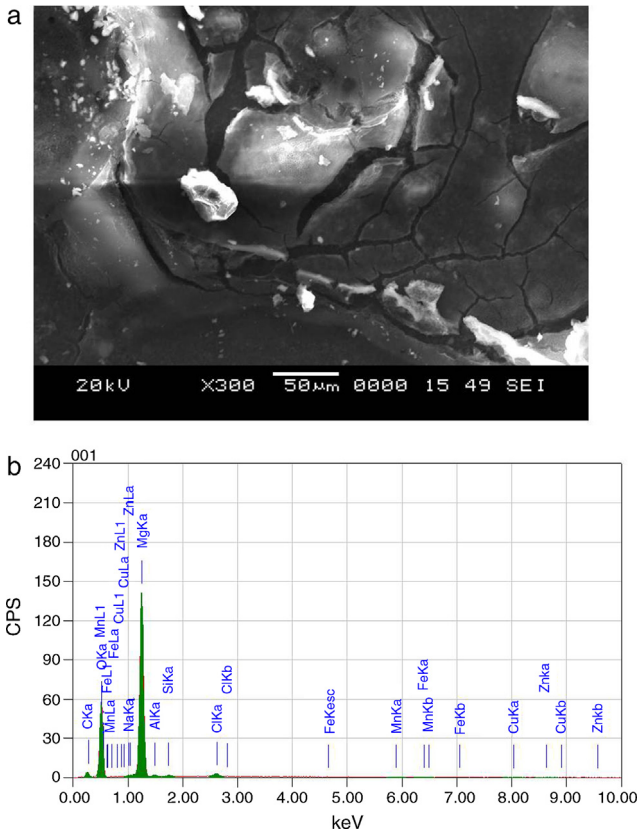

Fig. 13 – (a) SEM image and (b) EDX spectrum of the corroded surface of Mg–Al–Zn–Mn alloy specimen after immersion in 30% aqueous ethylene glycol containing 10 mM chloride ion for 24 h.

EDX spectra. Fig. 11(a) represents the SEM image of the freshly polished surface of the alloy, after etching in acetic-picral. The corresponding EDX spectra is presented in Fig. 11(b). The distribution of elements of Mg–Al–Zn–Mn alloy was determined using EDX mapping and is as shown in Fig. 12. Mg–Al–Zn alloy shows a biphasic microstructure with α-Mg solid solution and a discontinuous precipitation in lamellar form of β-phase ($Mg_{17}Al_{12}$). Presence of aluminum and manganese results in the formation of $MnAl_2$ inclusions as shown in the SEM image (Fig. 11(a)) and the same is supported by the EDX spectra recorded at specified areas (Fig. 11(b)). The SEM image and EDX spectrum of the corroded alloy surface after 24 h of immersion are shown in Fig. 13(a) and (b), respectively. The surface of the alloy is corroded with the formation of grooves and discontinuities. A strong peak of oxygen in the EDX pattern provides the proof for the proposed corrosion mechanism, with the formation of $Mg(OH)_2$.

4. Conclusions

Based on the results of the investigation, the following conclusions are drawn:

1. The corrosion rate of Mg–Al–Zn–Mn alloy is remarkably influenced by the environmental factors like temperature and chloride ions concentration.
2. Corrosion rate of Mg–Al–Zn–Mn alloy increases with the increase in temperature and chloride ion concentration.
3. The results of electrochemical analyses and surface analyses suggest the formation of partially protective $Mg(OH)_2$ film on the corroding alloy surface.
4. The corrosion kinetics follows Arrhenius law.

Conflicts of interest

The authors declare no conflicts of interest.

REFERENCES

[1] Song GL, Atrens A. Corrosion mechanisms of magnesium alloys. Adv Eng Mater 1999:11–33.
[2] Pardo A, Merino MC, Coy AE, Arrabal R, Viejo F, Matykina E. Corrosion behaviour of magnesium/aluminium alloys in 3.5 wt.% NaCl. Corros Sci 2008;50:823–34.
[3] Gupta M, Sharon NML. Magnesium, magnesium alloys and magnesium composites. John Wiley & Sons; 2011.
[4] Guo KW. A review of magnesium/magnesium alloys corrosion and its protection. Recent Pat Corros Sci 2010;2:13–21.
[5] Zeng R, Zhang J, Huang W, Dietzel W, Kainer KU, Blawert C, et al. Review of studies on corrosion of magnesium alloys. Trans Nonferr Met Soc China 2006;16 Suppl. 2:s763–71.
[6] Revie RW, Uhlig HH. Corrosion and corrosion control. John Wiley & Sons; 2008.
[7] Song G, Bowles AL, StJohn DH. Corrosion resistance of aged die cast magnesium alloy AZ91D. Mater Sci Eng A 2004;366:74–86.
[8] Blawert C, Dietzel W, Ghali E, Song G. Anodizing treatments for magnesium alloys and their effect on corrosion resistance in various environments. Adv Eng Mater 2006;8:511–33.
[9] Fan Y, Wu G, Zhai C. Influence of cerium on the microstructure, mechanical properties and corrosion resistance of magnesium alloy. Mater Sci Eng A 2006;433:208–15.
[10] Abbas G, Liu Z, Skeldon P. Corrosion behaviour of laser-melted magnesium alloys. Appl Surf Sci 2005;247:347–53.
[11] Tian XB, Wei CB, Yang SQ, Fu RKY, Chu PK. Corrosion resistance improvement of magnesium alloy using nitrogen plasma ion implantation. Surf Coat Technol 2005;198:454–8.
[12] Barchiche C-E, Rocca E, Juers C, Hazan J, Steinmetz J. Corrosion resistance of plasma-anodized AZ91D magnesium alloy by electrochemical methods. Electrochim Acta 2007;53:417–25.
[13] Song G, Atrens A, Wu X, Zhang B. Corrosion behaviour of AZ21, AZ501 and AZ91 in sodium chloride. Corros Sci 1998;40:1769–91.
[14] Bonora PL, Andrei M, Eliezer A, Gutman EM. Corrosion behaviour of stressed magnesium alloys. Corros Sci 2002;44:729–49.
[15] Chen J, Wang J, Han E, Dong J, Ke W. Corrosion behavior of AZ91D magnesium alloy in sodium sulfate solution. Mater Corros 2006;57:789–93.
[16] Badawy WA, Hilal NH, El-Rabiee M, Nady H. Electrochemical behavior of Mg and some Mg alloys in aqueous solutions of different pH. Electrochim Acta 2010;55:1880–7.
[17] Wang L, Shinohara T, Zhang B-P. Influence of chloride, sulfate and bicarbonate anions on the corrosion behavior of AZ31 magnesium alloy. J Alloys Compd 2010;496:500–7.

Please cite this article in press as: Medhashree H, Shetty AN. Electrochemical corrosion study of Mg–Al–Zn–Mn alloy in aqueous ethylene glycol containing chloride ions. J Mater Res Technol. 2016. http://dx.doi.org/10.1016/j.jmrt.2016.04.003

[18] Song G, Atrens A, John DS, Wu X, Nairn J. The anodic dissolution of magnesium in chloride and sulphate solutions. Corros Sci 1997;39:1981–2004.
[19] Zhang T, Shao Y, Meng G, Wang F. Electrochemical noise analysis of the corrosion of AZ91D magnesium alloy in alkaline chloride solution. Electrochim Acta 2007;53:561–8.
[20] Jamali SS, Moulton SE, Tallman DE, Forsyth M, Weber J, Wallace GG. Evaluating the corrosion behaviour of magnesium alloy in simulated biological fluid by using SECM to detect hydrogen evolution. Electrochim Acta 2015;152:294–301.
[21] Song G, StJohn D. Corrosion behaviour of magnesium in ethylene glycol. Corros Sci 2004;46:1381–99.
[22] Slavcheva E, Schmitt G. Screening of new corrosion inhibitors via electrochemical noise analysis. Mater Corros 2002;53:647–55.
[23] Fekry AM, Fatayerji MZ. Electrochemical corrosion behavior of AZ91D alloy in ethylene glycol. Electrochim Acta 2009;54:6522–8.
[24] Huang D, Hu J, Song G-L, Guo X. Inhibition effect of inorganic and organic inhibitors on the corrosion of Mg–10Gd–3Y–0.5Zr alloy in an ethylene glycol solution at ambient and elevated temperatures. Electrochim Acta 2011;56:10166–78.
[25] Slavcheva E, Petkova G, Andreev P. Inhibition of corrosion of AZ91 magnesium alloy in ethylene glycol solution in presence of chloride anions. Mater Corros 2005;56:83–7.
[26] Vander Voort G, Van Geertruyden W, Dillon S, Manilova E. Metallographic preparation for electron backscattered diffraction. Microsc Microanal 2006;12:1610–1.
[27] Zhao M-C, Liu M, Song G-L, Atrens A. Influence of pH and chloride ion concentration on the corrosion of Mg alloy ZE41. Corros Sci 2008;50:3168–78.
[28] Wang N, Wang R, Peng C, Feng Y, Zhang X. Corrosion behavior of Mg–Al–Pb and Mg–Al–Pb–Zn–Mn alloys in 3.5% NaCl solution. Trans Nonferr Met Soc China 2010;20:1936–43.
[29] Dinodi N, Nityananda Shetty A. Electrochemical investigations on the corrosion behaviour of magnesium alloy ZE41 in a combined medium of chloride and sulphate. J Magnes Alloy 2013;1:201–9.
[30] Fontana MG, Greene ND. Corrosion engineering. New York: McGraw-Hill Book Company; 1987. p. 8–29.
[31] Wei Guo K. A review of magnesium/magnesium alloys corrosion. Recent Pat Corros Sci 2011;1:72–90.
[32] Baghni M, Wu Y, Li J, Zhang W. Corrosion behavior of magnesium and magnesium alloys. Trans Nonferr Met Soc China 2004;14:1–10.
[33] Udhayan R, Bhatt DP. On the corrosion behaviour of magnesium and its alloys using electrochemical techniques. J Power Sources 1996;63:103–7.
[34] Natta MGL-B. Evidence of two anodic processes in the polarization curves of magnesium in aqueous media. Corrosion 2001;57:712–20.
[35] Froes FH, Eliezer D, Aghion E. The science, technology, and applications of magnesium. JOM 1998;50:30–4.
[36] Song G, Atrens A, Dargusch M. Influence of microstructure on the corrosion of diecast AZ91D. Corros Sci 1998;41:249–73.
[37] Zhao M-C, Liu M, Song G, Atrens A. Influence of the β-phase morphology on the corrosion of the Mg alloy AZ91. Corros Sci 2008;50:1939–53.
[38] Ambat R, Aung NN, Zhou W. Evaluation of microstructural effects on corrosion behaviour of AZ91D magnesium alloy. Corros Sci 2000;42:1433–55.
[39] Ambat R, Aung NN, Zhou W. Studies on the influence of chloride ion and pH on the corrosion and electrochemical behaviour of AZ91D magnesium alloy. J Appl Electrochem 2000;30:865–74.
[40] Aung NN, Zhou W. Effect of heat treatment on corrosion and electrochemical behaviour of AZ91D magnesium alloy. J Appl Electrochem 2002;32:1397–401.
[41] Jonsson M, Persson D, Gubner R. The initial steps of atmospheric corrosion on magnesium alloy AZ91D. J Electrochem Soc 2007;154:C684–91.
[42] Wu G, Fan Y, Gao H, Zhai C, Zhu YP. The effect of Ca and rare earth elements on the microstructure, mechanical properties and corrosion behavior of AZ91D. Mater Sci Eng A 2005;408:255–63.
[43] Fan Y, Wu G, Gao H, Li G, Zhai C. Influence of lanthanum on the microstructure, mechanical property and corrosion resistance of magnesium alloy. J Mater Sci 2006;41:5409–16.
[44] Carlson BE, Jones JW. The metallurgical aspects of the corrosion behaviour of cast Mg–Al alloys. In: Light Metals Processing and Applications Proceedings of the METSOC Conference. 1993. p. 833–47.
[45] Polmear IJ. Physical metallurgy of magnesium alloys. Magnesium alloys and their applications; 1992. p. 201–12.
[46] Gurrappa I. Characterization of titanium alloy Ti–6Al–4V for chemical, marine and industrial applications. Mater Charact 2003;51:131–9.
[47] Li T, Zhang H, He Y, Wang X. Comparison of corrosion behavior of Mg–1.5Zn–0.6Zr and AZ91D alloys in a NaCl solution. Mater Corros 2015;66:7–15.
[48] Perez N. Electrochemistry and corrosion science. Springer Science & Business Media; 2004.
[49] Heakal FE-T, Shehata OS, Tantawy NS. Enhanced corrosion resistance of magnesium alloy AM60 by cerium(III) in chloride solution. Corros Sci 2012;56:86–95.
[50] Dinodi N, Shetty AN. Alkyl carboxylates as efficient and green inhibitors of magnesium alloy ZE41 corrosion in aqueous salt solution. Corros Sci 2014;85:411–27.
[51] Wu G, Zhang X, Zhao Y, Ibrahim JM, Yuan G, Chu PK. Plasma modified Mg–Nd–Zn–Zr alloy with enhanced surface corrosion resistance. Corros Sci 2014;78:121–9.
[52] Song G-L, Xu Z. Crystal orientation and electrochemical corrosion of polycrystalline Mg. Corros Sci 2012;63:100–12.
[53] Fletcher S. Tables of degenerate electrical networks for use in the equivalent-circuit analysis of electrochemical systems. J Electrochem Soc 1994;141:1823–6.
[54] Zucchi F, Grassi V, Frignani A, Monticelli C, Trabanelli G. Electrochemical behaviour of a magnesium alloy containing rare earth elements. J Appl Electrochem 2005;36:195–204.
[55] Pebere N, Riera C, Dabosi F. Investigation of magnesium corrosion in aerated sodium sulfate solution by electrochemical impedance spectroscopy. Electrochim Acta 1990;35:555–61.
[56] Bentiss F, Lebrini M, Lagrenee M. Thermodynamic characterization of metal dissolution and inhibitor adsorption processes in mild steel/2,5-bis(n-thienyl)-1,3,4-thiadiazoles/hydrochloric acid system. Corros Sci 2005;47:2915–31.

Please cite this article in press as: Medhashree H, Shetty AN. Electrochemical corrosion study of Mg–Al–Zn–Mn alloy in aqueous ethylene glycol containing chloride ions. J Mater Res Technol. 2016. http://dx.doi.org/10.1016/j.jmrt.2016.04.003